Published in final edited form as:
Colloids Surf B Biointerfaces. 2014 April 1; 116: 452–458. doi:10.1016/j.colsurfb.2014.01.022.

Low-Dose Chemotherapy of Hepatocellular Carcinoma through Triggered-Release from Bilayer-Decorated Magnetoliposomes

Yanjing Chen[a], **Yuan Chen**[b], **Da Xiao**[b], **Arijit Bose**[a], **Ruitang Deng**[b], and **Geoffrey D. Bothun**[a,*]

[a]Department of Chemical Engineering, University of Rhode Island, 16 Greenhouse Road, Kingston, RI 02881, United States

[b]Department of Biomedical and Pharmaceutical Sciences, University of Rhode Island, 41 Lower College Road, Kingston, RI 02881, United State

Abstract

Low-dose (LD) chemotherapy is a promising treatment strategy that may be improved by controlled delivery. Polyethylene glycol-stabilized bilayer-decorated magnetoliposomes (dMLs) have been designed as a stimuli-responsive LD chemotherapy drug delivery system and tested *in vitro* using Huh-7 hepatocellular carcinoma cell line. The dMLs contained hydrophobic superparamagnetic iron oxide nanoparticles within the lipid bilayer and doxorubicin hydrochloride (DOX, 2 μM) within the aqueous core. Structural analysis by cryogenic transmission electron microscopy and dynamic light scattering showed that the assemblies were approximately 120 nm in diameter. Furthermore, the samples consisted of a mixture of dMLs and bare liposomes (no nanoparticles), which provided dual burst and spontaneous DOX release profiles, respectively. Cell viability results show that the cytotoxicity of DOX-loaded dMLs was similar to that of bare dMLs (~10%), which indicates that spontaneous DOX leakage had little cytotoxic effect. However, when subjected to a physiologically acceptable radiofrequency (RF) electromagnetic field, cell viability was reduced up to 40% after 8 h and complete cell death was observed after 24 h. The therapeutic mechanism was intracellular RF-triggered DOX release from the dMLs and not intracellular hyperthermia due to nanoparticle heating via magnetic losses.

Keywords

magnetoliposome; SPIO nanoparticle; hepatocellular carcinoma; drug delivery; magnetic nanoparticle; stimuli responsive

*Corresponding author: bothun@egr.uri.edu, +1-401-874-9518 (tel), +1-401-874-4689.

1. Introduction

Hepatocellular carcinoma (HCC) is the fifth most common cancer and the third most common cause of cancer-related death in the world [1]. HCC is resistant to chemotherapies, due in part to a number of drug resistance mechanisms, and systemic chemotherapy is generally ineffective [2]. When chemotherapies are used, high-dose (HD) therapies that induce apoptosis are commonly employed. It is common practice in most chemotherapies to use the highest possible dose. In contrast, low-dose (LD) therapies (also referred to as metronomic) can also be effective, while reducing undesirable patient side effects [3]. HD and LD therapies of doxorubicin hydrochloride (DOX) have recently been compared using the Huh-7 hepatocellular carcinoma cell line [4, 5]. For HD at 18.4 μM DOX, 6 days of treatment led to complete cell death *via* apoptosis. In contrast, LD at 92 nM DOX reduced cell viability from 100% to 85% after 6 days of treatment. While this reduction was modest, the cells eventually died through abnormal mitosis, rather than apoptosis, which was described as mitotic catastrophe were multiple micronuclei formed and there was a loss in membrane integrity [4].

A challenge to all chemotherapies is to increase the efficiency of treatment and minimize off-target side effects [6, 7]. As illustrated for HCC, overcoming drug resistance mechanisms and providing sustained LD therapies can help address this challenge. In the last decade, there has been significant activity in designing nanoscale drug delivery systems for targeted, controlled release [8–11]. The ideal system would be biocompatible, would achieve high drug encapsulation efficiency, would retain the drug until a target site is reached (i.e. not leaky), and would have high *in vivo* stability. One way to control when a drug is released, and its release rate, is to utilize a stimuli-responsive trigger [11–13].

Magnetoliposomes, which formed by encapsulating iron oxide nanoparticles within liposomes, have attracted interest as controlled release drug delivery agents due to their ability to change structure and permeability under low frequency magnetic fields [14–17]. A new method of magnetoliposome formation was introduced by Chen et al. where controlled release was achieved using bilayer-embedded hydrophobic superparamagnetic iron oxide (SPIO) nanoparticles and alternating electromagnetic fields operating at radio frequencies (RF) [18]. The liposomes were referred to as decorated magnetoliposomes or dMLs. The initial release rate and extent of release of an encapsulated dye was dependent upon the nanoparticle loading and the RF field strength. A unique aspect of the dMLs was that greater nanoparticle loading within the bilayer reduced spontaneous liposome leakage. Amstad et al. have since shown that incorporating a polyethylene glycol (PEG) lipid into dMLs can improve their colloidal stability and release properties [19]. They have also shown that the dMLs stayed intact through electromagnetic heating (i.e. the nanoparticles remained embedded within the bilayer).

Previous work has shown that dMLs can retain their cargo, including DOX, until triggered to release [18–20]. We hypothesize that this ability, coupled with the fact that dMLs are composed of biocompatible lipids and iron oxide nanoparticles, makes dMLs an interesting approach to HCC chemotherapy. The goal of this work is to demonstrate LD therapy and triggered-release *in vitro* using dMLs stabilized with PEG lipid. *In vitro* studies were

conducted with Huh-7 cell line and non-targeted dMLs. Cellular uptake was also confirmed in HEK-293 human embryonic kidney, SKRB3 human breast, and CV-1 monkey kidney cell lines. Experiments were conducted with and without RF exposure to differentiate between treatment due to passive DOX diffusion and triggered DOX release.

2. Materials and methods

2.1. Materials

SPIO maghemite nanoparticles (5 nm, 30 mg/mL or 187.9 mM Fe_2O_3) dispersed in chloroform were purchased from Ocean Nanotech (Springdale, AR). On the basis of the density of maghemite (4.9 g/cm^3), 30 mg ml^{-1} is equivalent to 9.4×10^{16} particles/mL. Dipalmitoylphosphatidylcholine (DPPC) in chloroform (20 mg/mL), dipalmityolphosphatidylethanolamine-N-(lissamine rhodamine B sulfonyl) (Liss Rhod PE) in chloroform (1 mg/mL) and dipalmitoylphosphatidylethanolamine-N-[methoxy(polyethylene glycol)-750] (PEG_{750}-PE) in chloroform (1 mg/mL) were purchased from Avanti Polar Lipids (Alabaster, AL), and DOX was purchased from Sigma Aldrich (St. Louis, MO). Phosphate buffered saline (PBS, pH 7.4) was prepared at 137 mM. Sterile deionized ultrafiltered (DI) water at 18.2 mΩ resistivity was used from a Millipore Direct-Q3 UV purification system (Billerica, MA). Dimethyl sulfoxide (DMSO) was purchased from Research Organics (Cleveland, OH). (4,5-dimethylthiazolyl-2)-2,5-diphenyltetrazolium bromide (MTT) assay was purchased from CALBIOCHEM (Billerica, MA).

Huh-7 hepatocellular carcinoma cancer cell line from ATCC (Manassas, VA) was used in the *in vitro* study. Dulbecco's modified Eagle medium (DMEM) and fetal bovine serum (FBS) were purchased from LONZA (Allendale, NJ). Penicillin/streptomycin, and non-essential amino acids (NEAA) were purchased from Biowhittaker (Radnor, PA). Trypsin was purchased from Gibco (Grand Island, NY).

2.2. Preparation of dMLs and DOX–loaded dMLs

dMLs were prepared at 5 mM total lipid and at lipid molecule to nanoparticle ratio of 10,000:1 (L/N, molar ratio) by a modified reverse phase evaporation (REV) method. The lipid composition was DPPC/PEG_{750}-PE at molar r atio of 95:5, respectively. In this process, aliquots of the lipids and SPIO NPs dissolved in chloroform were pipetted into a round-bottom flask to provide the desired composition and mixed with PBS. Chloroform was removed by rotary evaporation at 50 °C (above the DPPC melting temperature) starting at 450 mbar for 30 min, then decreased to 300 mbar for 30 min, and finally 200 mbar for 30 min. Additional PBS was added into final solution to desired volume. Then samples were extruded through double-stacked polycarbonate membranes with 100 nm pore diameters.

DOX was encapsulated at 2 μM and unencapsulated DOX was removed from DOX-dMLs by dialysis for 24 h using 1,000 kDa tubular cellulose acetate membranes (Sigma, St. Louis, MO) with stirring and frequent media exchange. Washing solution containing unencapsulated DOX was collected and analyzed by fluorescence spectroscopy (Perkin-Elmer LS 55) to determine encapsulation efficiency. Based on a mass balance of DOX, 97%

of the initial unencapsulated DOX was removed by dialysis. All samples were used within 2 days of preparation.

2.3. Characterization of dMLs

Dynamic light scattering (DLS) measurements were made using a Malvern Instruments Zetasizer Nano ZS with a backscattering detector angle of 173° and a 4 mW, 633 nm He-Ne laser (Worcestershire, UK). To determine size distribution, dMLs samples were diluted 10-fold with DMEM and analyzed in an optical grade polystryrene cuvette at 37 °C. The reported z-averaged and intensity-weighted hydrodynamic diameters are based on 15 scans. After measurement, this sample was stored in water bath at 37 °C. To investigate the aggregation of dMLs, the size distribution was measured every two days and the average size was plot as a function of time.

Cryogenic transmission electron microscopy (cryo-TEM) samples were prepared at 37 °C using a Vitrobot (FEI Company, Hillsboro, OR), which is a PC-controlled robot for sample vitrification. Quantifoil grids were used with 2 μm carbon holes on 200 square mesh copper grids (Electron Microscopy Sciences, Hatfield, PA). To prepare a sample, it was first equilibrated within the Vitrobot chamber at 37 °C and 100% humidity for 30 min. After immersing the grid into the sample, it was then removed, blotted to reduce film thickness, and vitrified in liquid ethane. The sample was then transferred to liquid nitrogen for storage. Imaging was performed in a cooled stage (model DH 926, Gatan Inc., Pleasanton, CA) at 200 kV using a JEOL JEM-2100 TEM (Peabody, MA). Size analysis was performed using ImageJ software [21]. Energy-dispersive X-ray spectroscopy or EDS (Model INCAx-act, Oxford Instruments, UK) was used to detect elemental iron from the SPIO nanoparticles within the dMLs. EDS was conducted during cryogenic imaging with 158 s of live time and 92 s of dead time.

2.4. *In situ* DOX release by dMLs

DOX release was examined *in situ* using a well-plate model in the absence of Huh-7 cells. DOX-dMLs were transferred to a 6-well culture plate at an effective DOX concentration of 100 nM. The plate was placed on a pancake-style copper heating coil (3 turns) and subjected to a RF field for 30 min that was generated by a 1 kW Hotshot (Ameritherm Inc., Scottsville, NY) operating at 250 A and 170 kHz (Figure 1). After heating, the samples were transferred to a 1,000 kD dialysis tube placed in a 80 mL dialysate beaker that was filled with DI water. The fluorescence intensity of DOX in the dialysate was measured as a function of time. Control experiments included DOX-dMLs without RF exposure and 100 nM of free DOX (no dMLs).

2.5. *In vitro* cellular uptake of dMLs

Huh-7 cell lines were incubated at 37 °C, under humidified air with 5% CO_2, in serum-free DMEM supplemented with 10% (v/v) FBS, 100 ug/mL per 100 ug/mL penicillin/ streptomycin, and 1% non-essential amino acids. Cells in maintenance medium were trypsinized and seeded into 6-well culture plates at optimum confluence. Incubations were conducted with dMLs at 0, 2, 5, 10, 20 and 40 μM total lipid in serum-containing maintenance medium for 24 h. For fluorescence imaging, Liss Rhod PE was added to the

dMLs at 0.1 mol%. After 24 h, the cells were washed with PBS to remove free dMLs. Cellular uptake of dMLs was monitored by fluorescence microscopy on an inverted Nikon microscope under 200× magnification and fluorescence intensity was measured using ImageJ. Uptake experiments were conducted in triplicate.

2.6. *In vitro* DOX release by dMLs

The diffusion of DOX in Huh-7 cells with and without RF exposure was tracked qualitatively by fluorescence microscopy. In this experiment, cells in seeded in a 6-well tissue culture plate were treated with DOX-dMLs for 1 h. After washing, a single cell colony with DOX-dMLs was imaged by bright field and fluorescence microscopy. The plates were then exposed to the RF field as previously described for *in situ* DOX release. The same cell colony was observed before and after RF exposure, and DOX diffusion was tracked qualitatively by comparing the fluorescence intensities. Cells treated with DOX-dMLs without RF exposure served as the control. *In situ* temperature measurements were conducted by inserting a fiber optic temperature probe (LumaSense Technologies, Inc., Santa Clara, CA) into the cell culture media.

2.7. Cell Viability Assay

The cytotoxicity of dMLs and DOX-loaded dMLs (DOX-dMLs) was determined by MTT assay. Briefly, Huh-7 cells were plated to clear-bottomed 96-well tissue culture plates at a density of 5×10^4 cells per well 24 h prior to the assay. The culture medium on the well was replaced with 100 μL of fresh medium containing dMLs or DOX-dMLs. The assay was conducted by adding 10 μL of 5 mg/mL MTT dissolved in PBS to each well and incubating for 3 h at 37 °C. The medium was then removed and the resulting MTT formazan was solubilized in 100 μL of DMSO. The number of viable cells in each well was then determined by measuring the absorbance of the samples at 570 nm with reference wavelength of 690 nm on an automated plate reader.

The viability of Huh-7 cells treated with DOX-dMLs was also examined with RF exposure to mirror the *in vitro* DOX release experiment. In this experiment, the cells were incubated with DOX-dMLs for 3 h, after which the media in each well was removed and the cells were washed three times with fresh media. The cells were exposed to RF for 30 min RF followed by 8 h incubation period, after which the MTT assay was conducted. Cells treated with DOX-dMLs without exposure RF were included as controls.

3. Results and discussion

3.1. dML Assembly and Characterization

dML assembly was driven by hydrophobic interactions between the SPIO nanoparticle oleic acid coating and the lipid acyl tails. Cryo-TEM, EDS, and DLS were used to verify dML size and nanoparticle loading (Figure 2). The representative micrograph shows uniform structures with no evidence of dML aggregation. The sample consisted of dMLs containing SPIO nanoparticle clusters (black arrows; Figure 2B) and what appear to be bare liposomes (white arrow; Figure 2B). This is depicted schematically in Figure 2A. Nanoparticle clustering within the bilayer, as opposed to being dispersed spatially, reflects the

configuration that minimizes the elastic energy penalty associated with the bilayer leaflets "wrapping" around the nanoparticles [22]. The bare liposomes could simply contain low nanoparticle loadings, but it was not possible to confirm this based on the micrographs. In both cases the assemblies were faceted and polygonal in shape, which is consistent with solid bilayer sheets meeting at defects in rigid gel phase liposomes [23, 24]. Nanoparticle loading within the dMLs was verified qualitatively by detecting elemental iron (Fe) using EDS (Figure 2C). Characteristic K_α and K_β peaks for Fe were observed near 6.4 and 6.9 keV, respectively. Nanoparticles were not detected outside of the dMLs based on random EDS mapping (results not shown). The average size of dMLs was 118 ± 26 nm, which was consistent with the DLS results (Figure 2D).

DLS was conducted in cell culture medium; DMEM supplemented with FBS. The results show the average hydrodynamic diameter of the dMLs remained between 117 nm and 140 nm over 6 days (Figure 2D). Between day 6 and day 8 the hydrodynamic diameter increased to 179 nm. The associated polydispersity indices for the entire timescale ranged from 0.16 to 0.18, which suggests that the dMLs remained monodispersed and did not appreciably aggregate in the presence of serum protein. This was confirmed by visual inspection and expected based on steric repulsion provided by the PEG lipid. At the concentration employed (5 mol%), PEG_{750} extended 1.9 nm from the liposome surface in a mushroom configuration [20, 25]. The PEG molecular weight could have been increased to enhance steric repulsion, however, increasing PEG molecular weight has been shown to increase spontaneous liposome leakage, which is obviously undesirable for our purposes [26].

DOX release was examined with and without 30 min of initial RF exposure in a 6-well plate (Figure 3). After exposure the samples were transferred to dialysis tubes and the dialysate was analyzed for DOX concentration over 24 h. An equivalent free DOX concentration was used as a control. Free DOX rapidly diffused through the dialysis membranes and quickly equilibrated with the dialysate near 100 nM. dMLs without RF exposure yielded a steady increase in DOX dialysate concentration over 24 h, which can be attributed to passive or spontaneous DOX leakage from dMLs. Comparatively, the initial increase in DOX dialysate concentration with RF exposure was significantly greater due to the RF-triggered release of free DOX in the sample (Figure 3, inset). After RF exposure, there was a steady increase in DOX dialysate concentration from 30 min to 24 h. These results are consistent with a burst-release mechanism by RF exposure of dMLs, followed by passive DOX leakage.

3.2. Cellular uptake of dMLs

Corresponding bright field and fluorescence images of cellular uptake by Huh-7 as a function of dML lipid concentration (5 μM, 20 μM, and 40 μM) are shown in Figure 4. The cells were incubated with dMLs for 24 h and washed before imaging. dMLs were not observed outside of cells, indicating that free dMLs were removed by washing. Fluorescence intensity increased linearly with dML lipid concentration suggesting a direct proportionality between uptake and lipid concentration (Figure 4D; $R^2 = 0.977$). Cellular uptake was also examined as a function of time (1, 2, and 3 h) at 5 μM and 20 μM dML concentrations (Figure 4E). Based on a linear relationship between fluorescence intensity and time, the uptake rate at 20 μM was 1.7-fold greater than at 5 μM dML concentration. It is well known

that small vesicles such as the dMLs (~100 nm in diameter) enter cells through endocytosis [27, 28]. Uptake was likely controlled by dML diffusion to the cell surface given that the dMLs w ere non-targeting, and the linear relationships between fluorescence intensity, dML concentration, and time. In addition, an order of magnitude estimate of diffusion time of dMLs over an average intracellular distance is ~10^4 s, consistent with the time scales for fluorescence intensity increase reported here.

3.3. Cell viability and dML treatment

Drug delivery systems should have minimal cytotoxicity during circulation in vivo. Results of the MTT assay showed a 10% decrease in relative cell viability after 24 h incubation at the highest dML lipid concentration (40 μM; Figure 5A). This shows that the dMLs (no DOX) had minimal cytotoxicity to Huh-7 cells at the conditions examined.

The cytotoxicity of DOX-dMLs with and without RF exposure was conducted to identify the treatment mechanism (Figure 5B). Control experiments were conducted with DOX dissolved in PBS (free DOX) from 0.08 nM to 1.6 nM DOX, which was equivalent to the effective DOX concentration per sample volume at lipid concentrations from 2 μM to 40 μM, respectively. In these experiments, 98% cell viability was observed 8 h after DOX treatment at 1.6 nM DOX (results not shown). For DOX-dMLs without RF exposure, 76% cell viability was observed at the highest lipid concentration (40 μM) which significantly less than that for bare dMLs and free DOX. Hence, DOX is cytotoxic at the concentrations employed only when delivered by dMLs. With RF exposure (30 min following 3 h incubation), there was a clear decrease in cell viability at all dML concentrations compared to no RF exposure. The viability of Huh-7 cells decreased linearly with lipid concentration to 62% at a lipid concentration of 40 μM. It is important to note that a field strength Hf (H is the amplitude and f is the frequency of the RF field) of 7.1×10^4 kA m^{-1} s^{-1} was used in this study, well below the physiological t olerance limit of 4.85×10^5 kA m^{-1} s^{-1} [29].

DOX release was further confirmed *in vitro*. Huh-7 cells with internalized DOX-dMLs at lipid concentrations of 5 μM (Figure 5C, 1–3) or 20 μM (Figure 5C, 4–6) were imaged before and after 30 min RF exposure. Before RF exposure there was little change in fluorescence for 3 h, which shows that the dMLs were stable and did not leak appreciably within the cells (Figure 5C, 2 and 5). After RF exposure the fluorescence weakened (white arrows; Figure 5C, 3 and 6) or disappeared (yellow arrows; Figure 5C, 3 and 6). At 5 μM and 20 μM lipid concentrations, fluorescence intensity was reduced by 79% and 56%, respectively. No change in fluorescence was observed for DOX-dMLs when RF exposure was not applied (results not shown). Reductions in fluorescence can be attributed to RF-triggered DOX release, due to bilayer permeabilization or disruption, which is consistent with our previous work [18].

Control experiments were conducted to assess the effects of the electromagnetic field (no dMLs), RF exposure alone with dMLs (no DOX; Figure 6), and potential temperature changes on cell viability. First, cell viability assays were performed in 96-well plates after the cells were subjected to 30 min in the electromagnetic field. Greater than 99% cell viability was measured, which confirms that the electromagnetic field alone did not affect cell viability. Second, cell viability assays were performed after the cells were subjected to

30 min RF exposure with dMLs. Cell viability was similar to that for bare dMLs, which shows that RF exposure alone (i.e. hyperthermia treatment) had a minor effect on cell viability relative to DOX delivery. Finally, temperature was measured in situ during the RF exposure experiments and the maximum temperature rise was 0.67 °C. Hence, cell death can be attributed solely to RF-triggered DOX release.

The rationale for choosing dMLs with hydrophobic SPIO nanoparticles as release-triggers was twofold. First, embedding hydrophobic nanoparticles places the trigger directly within the permeability (bilayer) barrier [18, 30, 31]. The exact mechanism of permeabilization is not known, but likely involves combined heat and mechanical disruption [11]. Second, it has been previously observed that embedding hydrophobic SPIO nanoparticle can reduce spontaneous leakage of an encapsulated dye molecule [18]. This observation has been verified *in vitro* for encapsulated DOX. By reducing spontaneous leakage, LD therapies become more feasible as the passive loss of cargo is reduced, which allows more cargo to be taken up by the cells.

Based on cryo-TEM analysis, the embedded nanoparticles (5 nm γ-Fe_2O_3 core) were not evenly distributed within the bilayer, but rather existed as aggregates or clusters. Rasch et al. and Von White et al. have observed similar behavior for small hydrophobic gold nanoparticles in lipid bilayers [22, 32]. Nanoparticle clustering minimizes the energy penalty associated with bilayer bending around the nanoparticles (i.e. it is more energetically more favorable to accommodate a single nanoparticle cluster than the nanoparticles individually that comprise that cluster). Despite nanoparticle clustering within the bilayers, the dMLs remained stable and retained their cargo until triggered to release.

Although DOX was encapsulated within the dMLs at 2 μM, the effective DOX concentration at 40 μM lipid was 1.6 nM. Comparatively, Park et al. reported that the viability of Huh-7 cells reduced to 85% after 6 days of treatment at 92 nM free DOX [4]. We observed a similar reduction in cell viability using RF-triggered DOX release at a lower effective DOX concentration after 8 h. Furthermore, we observed complete cell death with RF-triggered DOX release over the range of lipid concentrations from 5 to 40 μM after 24 h incubation (results not shown). For the same conditions without RF heating, live cells were detected at all but the highest lipid concentration (40 μM), and cell viability ranged from 16% to 35%. Comparatively, 98% cell viability was observed for the DOX control after 24 h at the equivalent dML concentrations.

4. Conclusions

Low-dose chemotherapy of Huh-7 cells was achieved by RF-triggered release of DOX from dMLs, where cellular uptake was governed by dML diffusion within the culture media consistent with a non-targeted delivery vehicle. The dMLs contained a mixed population of nanoparticle-loaded and bare liposomes, which provided two different release profiles (triggered and spontaneous). Control experiments confirmed that the cytotoxicity could be attributed to triggered drug release and not the RF-heating properties of the nanoparticles alone. These experiments were conducted in serum-containing media and that the presence of serum did not hinder cellular uptake or intracellular DOX release. Experiments are

currently underway to modify dML designs with targeting moieties and to examine dML release *in vivo*. Further modification to include targeting ligands would facilitate greater cellular uptake and cellular specificity [33].

Acknowledgments

This material is based upon work supported by the National Science Foundation under Grant No. CBET-0931875 and by the National Institute of Standards and Technologies under Grant No. 60NANB10D139.

References

1. Lodato F, Mazzella G, Festi D, Azzaroli F, Colecchia A, Roda E. Hepatocellular carcinoma prevention: A worldwide emergence between the opulence of developed countries and the economic constraints of developing nations. World J Gastroentero. 2006; 12:7239–7249.
2. Nowak AK, Chow PKH, Findlay M. Systemic therapy for advanced hepatocellular carcinoma: a review. Eur J Cancer. 2004; 40:1474–1484. [PubMed: 15196530]
3. Pasquier E, Kavallaris M, Andre N. Metronomic chemotherapy: new rationale for new directions. Nat Rev Clin Oncol. 2010; 7:455–465. [PubMed: 20531380]
4. Eom YW, Kim MA, Park SS, Goo MJ, Kwon HJ, Sohn S, Kim WH, Yoon G, Choi KS. Two distinct modes of cell death induced by doxorubicin: apoptosis and cell death through mitotic catastrophe accompanied by senescence-like phenotype. Oncogene. 2005; 24:4765–4777. [PubMed: 15870702]
5. Park SS, Kim MA, Eom YW, Choi KS. Bcl-xL blocks high dose doxorubicin-induced apoptosis but not low dose doxorubicin-induced cell death through mitotic catastrophe. Biochem Bioph Res Co. 2007; 363:1044–1049.
6. Immordino ML, Dosio F, Cattel L. Stealth liposomes: review of the basic science, rationale, and clinical applications, existing and potential. Int J Nanomed. 2006; 1:297–315.
7. Mishra B, Patel BB, Tiwari S. Colloidal nanocarriers: a review on formulation technology, types and applications toward targeted drug delivery. Nanomed-Nanotechnol. 2010; 6:9–24.
8. Gindy ME, Prud'homme RK. Multifunctional nanoparticles for imaging, delivery and targeting in cancer therapy. Expert Opin Drug Del. 2009; 6:865–878.
9. Phillips MA, Gran ML, Peppas NA. Targeted n anodelivery of drugs and diagnostics. Nano Today. 2010; 5:143–159. [PubMed: 20543895]
10. Petros RA, DeSimone JM. Strategies in the design of nanoparticles for therapeutic applications. Nat Rev Drug Discov. 2010; 9:615–627. [PubMed: 20616808]
11. Preiss MR, Bothun GD. Stimuli-responsive liposome-nanoparticle assemblies. Expert Opin Drug Del. 2011; 8:1025–1040.
12. Ganta S, Devalapally H, Shahiwala A, Amiji M. A review of stimuli-responsive nanocarriers for drug and gene delivery. J. Controlled Release. 2008; 126:187–204.
13. Vivero-Escoto JL, Slowing II, Wu CW, Lin VSY. Photoinduced Intracellular Controlled Release Drug Delivery in Human Cells by Gold-Capped Mesoporous Silica Nanosphere. J. Am. Chem. Soc. 2009; 131:3462. -+ [PubMed: 19275256]
14. Nappini S, Bonini M, Ridi F, Baglioni P. Structure and permeability of magnetoliposomes loaded with hydrophobic magnetic nanoparticles in the presence of a low frequency magnetic field. Soft Matter. 2011; 7:4801–4811.
15. Nappini S, Al Kayal T, Berti D, Norden B, Baglioni P. Magnetically Triggered Release From Giant Unilamellar Vesicles: Visualization By Means Of Confocal Microscopy. J Phys Chem Lett. 2011; 2:713–718.
16. Skouras A, Mourtas S, Markoutsa E, De Goltstein MC, Wallon C, Catoen S, Antimisiaris SG. Magnetoliposomes with high USPIO entrapping efficiency, stability and magnetic properties. Nanomed-Nanotechnol. 2011; 7:572–579.
17. Benyettou F, Chebbi I, Motte L, Seksek O. Magnetoliposome for alendronate delivery. J Mater Chem. 2011; 21:4813–4820.

18. Chen Y, Bose A, Bothun GD. Controlled Release from Bilayer-Decorated Magnetoliposomes via Electromagnetic Heating. ACS Nano. 2010; 4:3215–3221. [PubMed: 20507153]
19. Amstad E, Kohlbrecher J, Muller E, Schweizer T, Textor M, Reimhult E. Triggered Release from Liposomes through Magnetic Actuation of Iron Oxide Nanoparticle Containing Membranes. Nano Letters. 2011; 11:1664–1670. [PubMed: 21351741]
20. Bothun GD, Lelis A, Chen Y, Scully K, Anderson LE, Stoner MA. Multicomponent folate-targeted magnetoliposomes: design, characterization, and cellular uptake. Nanomed-Nanotechnol. 2011; 7:797–805.
21. Abramoff MD, Magelhaes PJ, Ram SJ. Image processing with ImageJ. Biophotonics Intl. 2004; 11:36–42.
22. Rasch MR, Rossinyol E, Hueso JL, Goodfellow BW, Arbiol J, Korgel BA. Hydrophobic Gold Nanoparticle Self-Assembly with Phosphatidylcholine Lipid: Membrane-Loaded and Janus Vesicles. Nano Lett. 2010; 10:3733–3739. [PubMed: 20731366]
23. Lichtenberg D, Freire E, Schmidt CF, Barenholz Y, Felgner PL, Thompson TE. Effect of surface curvature on stability, thermodynamic behavior, and osmotic activity of dipalmitoylphosphatidylcholine single lamellar vesicles. Biochemistry. 1981; 20:3462–3467. [PubMed: 6894860]
24. Dierksen K, Typke D, Hegerl R, Walz J, Sackmann E, Baumeister W. Three-dimensional structure of lipid vesicles embedded in vitreous ice and investigated by automated electron tomography. Biophys. J. 1995; 68:1416–1422. [PubMed: 7787027]
25. Hristova K, Needham D. The Influence of Polymer-Grafted Lipids on the Physical- Properties of Lipid Bilayers - a Theoretical-Study. J. Coll. Interfac. Sci. 1994; 168:302–314.
26. Sriwongsitanont S, Ueno M. Physicochemical properties of PEG-grafted liposomes. Chem Pharm Bull (Tokyo). 2002; 50:1238–1244. [PubMed: 12237543]
27. Sharma A, Sharma U. Liposomes in dru g delivery: progress and limitations. Int J Pharm. 1997; 154:123–140.
28. Ishida O, Maruyama K, Sasaki K, Iwatsuru M. Size-dependent extravasation and interstitial localization of polyethyleneglycol liposomes in solid tumor-bearing mice. Int J Pharm. 1999; 190:49–56. [PubMed: 10528096]
29. Brezovich IA, Atkinson WJ, Lilly MB. Local hyperthermia with interstitial techniques. Cancer Res. 1984; 44:4752s–4756s. [PubMed: 6380712]
30. Park S-H, Oh S-G, Mun J-Y, Hany S-S. Loading of gold nanoparticles inside the DPPC bilayers of liposome and their effects on membrane fluidities. Colloid. Surface. B. 2006; 48:112–118.
31. Paasonen L, Sipila T, Subrizi A, Laurinmaki P, Butcher SJ, Rappolt M, Yaghmur A, Urtti A, Yliperttula M. Gold-embedded photosensitive liposomes for drug delivery: Triggering mechanism and intracellular release. J. Control. Release. 2010; 147:136–143. [PubMed: 20624434]
32. Von White G II, Chen Y, Roder-Hanna J, Bothun GD, Kitchens CL. Structural and Thermal Analysis of Lipid Vesicles Encapsulating Hydrophobic Gold Nanoparticles. ACS Nano.
33. Mamot C, Drummond DC, Greiser U, Hong K, Kirpotin DB, Marks JD, Park JW. Epidermal growth factor receptor (EGFR)-targeted immunoliposomes mediate specific and efficient drug delivery to EGFR- and EGFRvIII-overexpressing tumor cells. Cancer Res. 2003; 63:3154–3161. [PubMed: 12810643]

Highlights

- Stimuli-responsive magnetoliposomes (dMLs) were designed for low dose chemotherapy.
- SPIO nanoparticles provided a bilayer trigger for intracellular doxorubicin release.
- High dML uptake was observed in Huh-7 cell line *in vitro*.
- dMLs exhibited low cytotoxicity unless activated by an external RF field.
- Huh-7 treatment was due to doxorubicin release and not local hyperthermia.

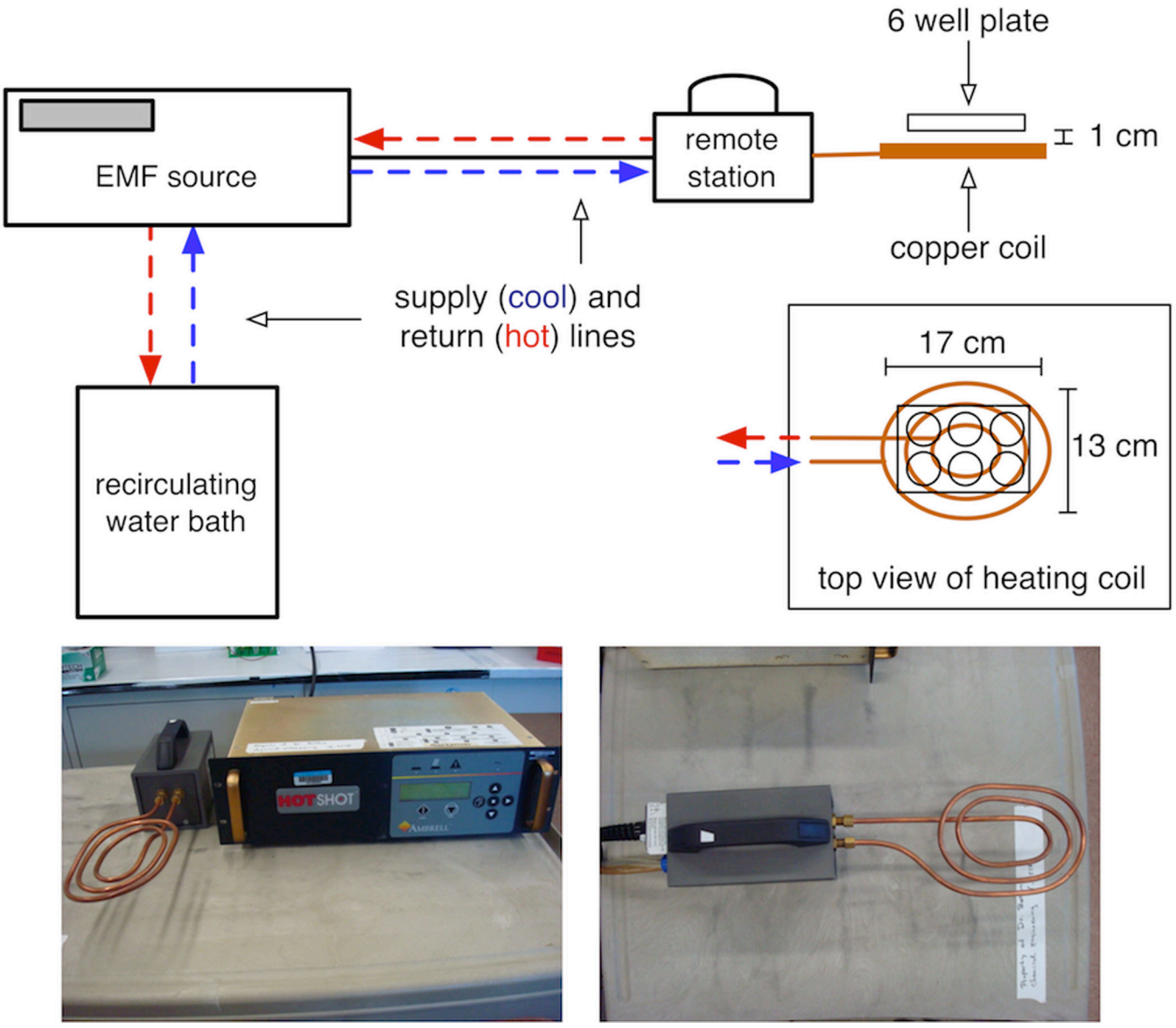

Figure 1.
The *in vitro* system for RF exposure.

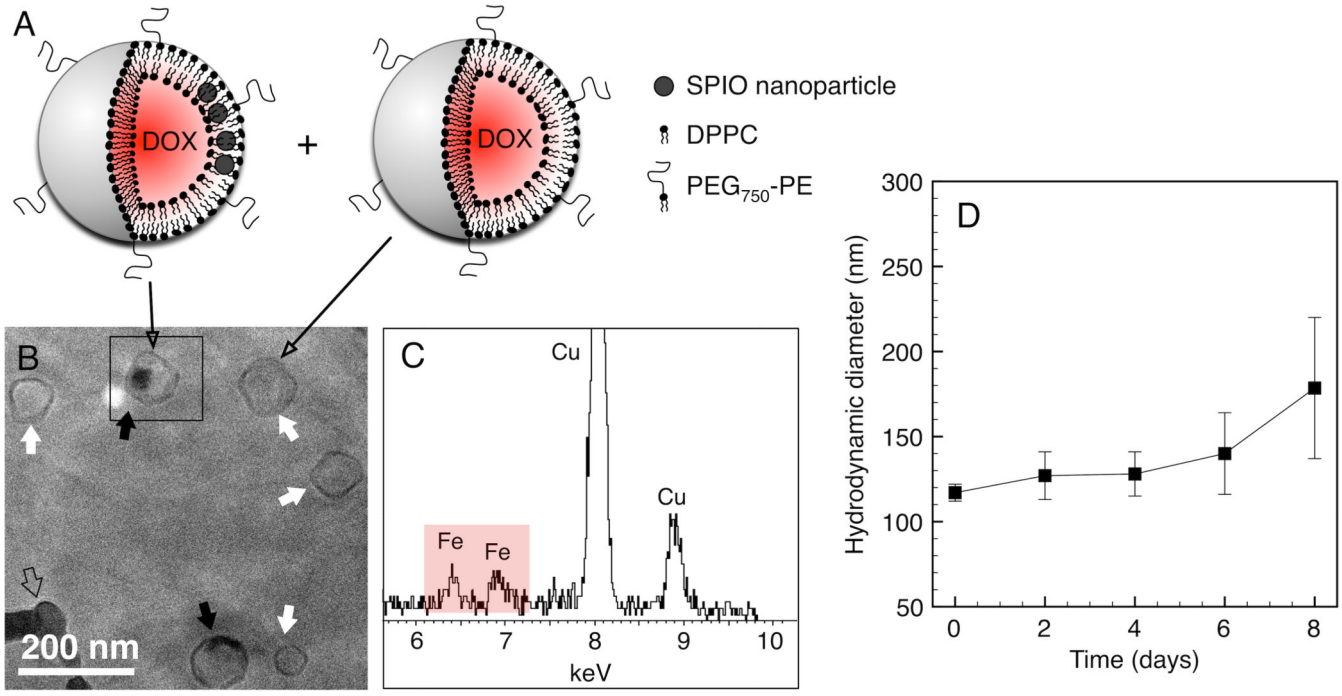

Figure 2.

Characterization of self-assembled dMLs. (A) Schematic depicting a sample population of dMLs and bare liposomes. (B) Cryo-TEM micrograph of dMLs in PBS water vitrified 1 day after preparation at 37 °C. Black arrows denote dMLs and white arrows denote bare liposomes. (C) EDS map for selected area in (A) confirms the presence of Fe from the nanoparticles. The open arrow denotes a frozen ethane artifact. (D) Hydrodynamic diameter of dMLs in FBS supplemented PBS as function of time determined by DLS. Error bars represent standard error for duplicate samples.

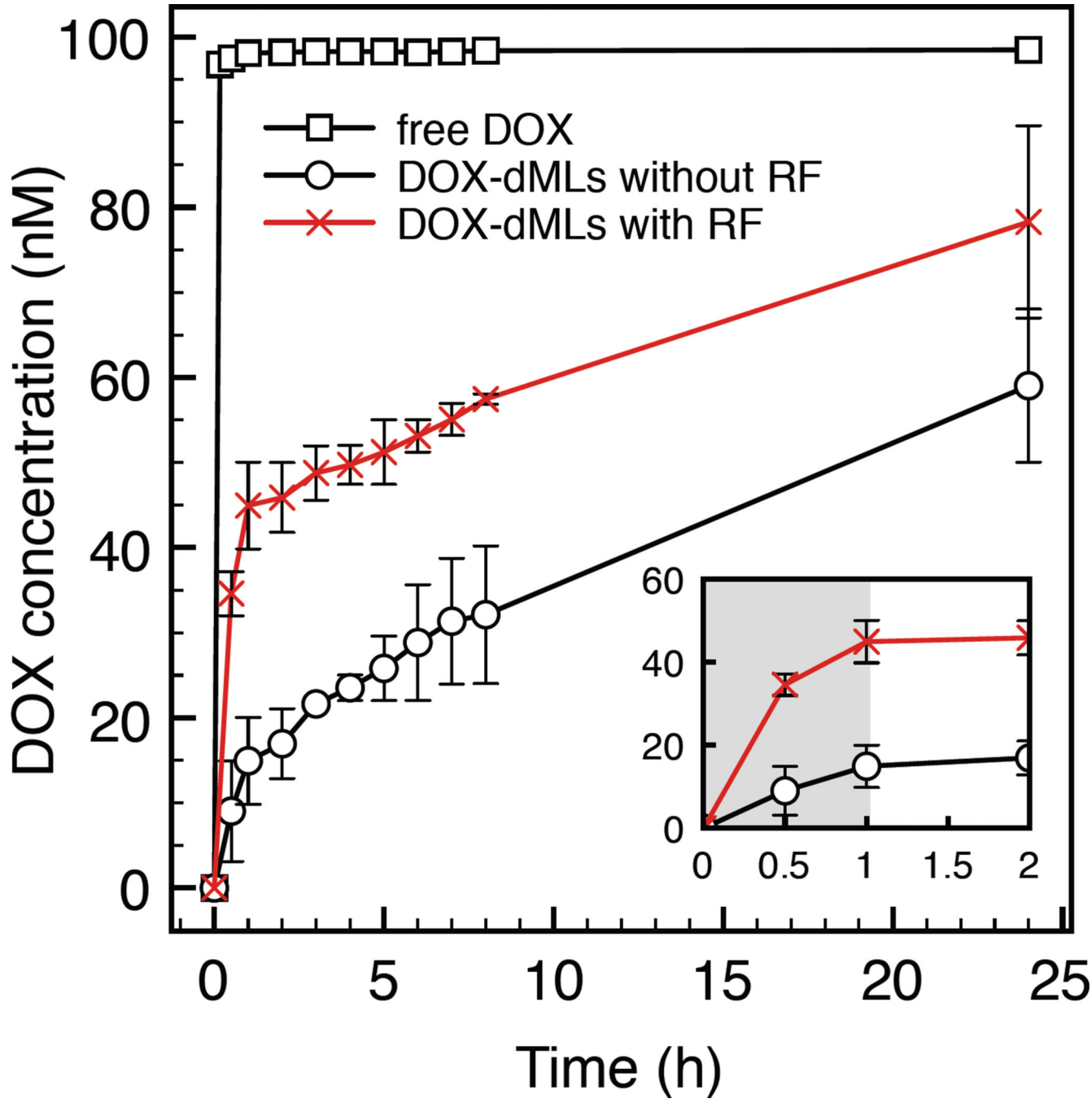

Figure 3.

DOX release as a function of time measured by dialysis. For the dML experiments, samples were placed in 6-well plates from 0 to 30 min (with or without RF exposure) and then transferred to dialysis tubes where the DOX concentration in the dialysate was measured. The inset shows the dialysate concentration at shorter times. Error bars represent standard error for duplicate samples.

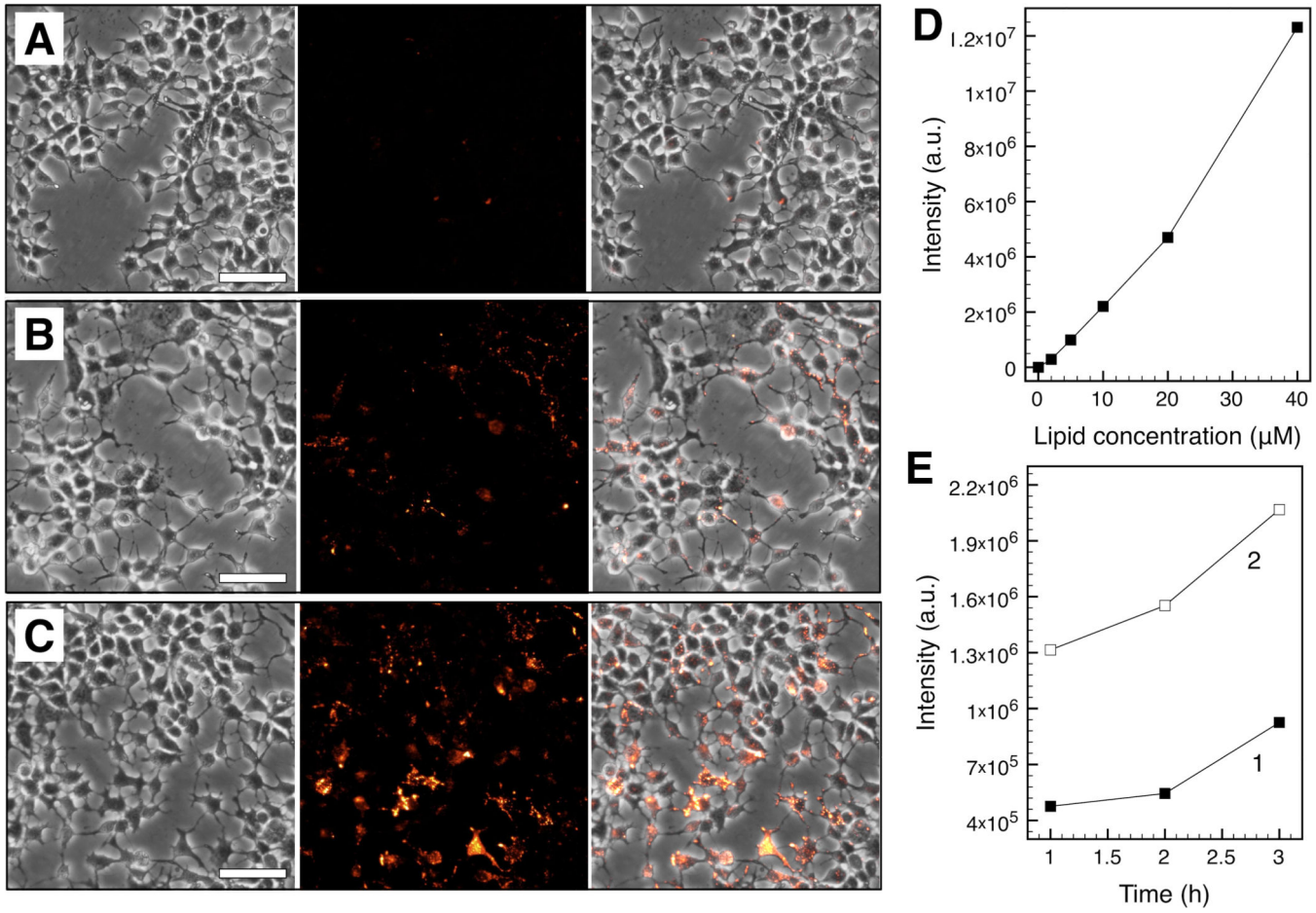

Figure 4.

In vitro dML uptake by Huh-7 cells after 24 h incubation. Corresponding bright field (left), fluorescence (middle), and merged brighfield-fluorescence (right) micrographs are shown at lipid concentrations of 5 μM (A), 20 μM (B), and 40 μM (C) (scale bar = 25 μm). Fluorescence stems from Liss Rhod PE incorporated within the dML bilayers. Total fluorescence intensity was determined from the micrographs (D) as a function of lipid concentration after 24 h incubation and (E) as a function of time at lipid concentrations of 5 μM (1) and 20 μM (2).

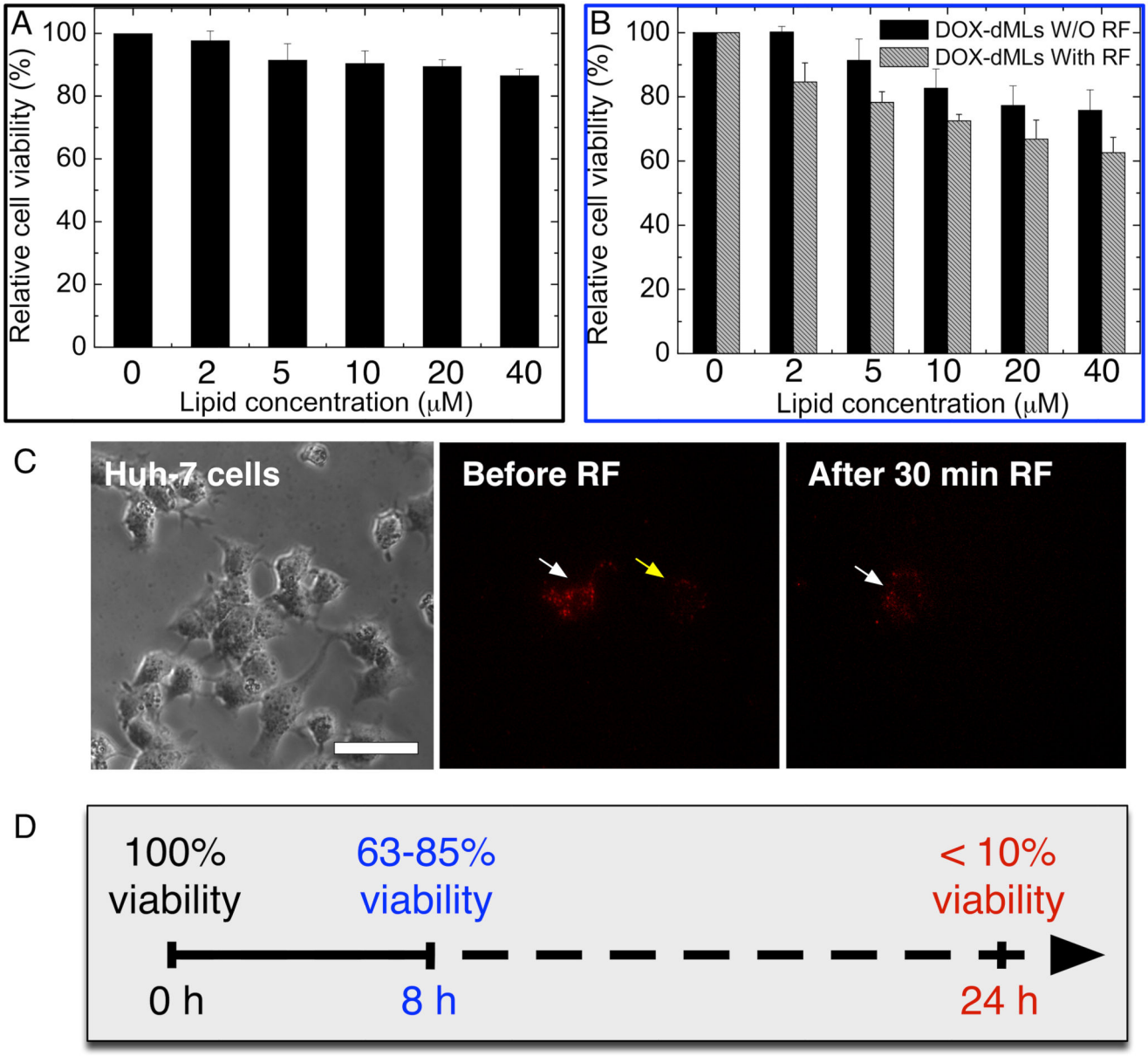

Figure 5.

In vitro cytotoxicity and treatment re sults from dMLs. (A) Cytotoxicity of bare dMLs (no DOX) evaluated by MTT assay after 24 h incubation. (B) Comparative cytotoxicity of DOX-loaded dMLs with and without RF exposure. For (B), the cells were incubated for 3 h with dMLs and exposed to 30 min of RF exposure. For both (A) and (B), the MTT assays were conducted after 8 h incubation following the treatment. Error bars represent standard deviation for n = 16. (C) Direct imaging of RF-induced DOX release *in vitro* (scale bar = 50 μm). Fluorescence stems from DOX encapsulated within dMLs. Bright field micrograph shows Huh-7 cells incubated with DOX-loaded dMLs at lipid concentrations of (1) 5 μM and (4) 20 μM. The fluorescence micrographs correspond to the treated cells before RF exposure (2, 5 μM) and F (5, 20 μM) and after 30 min RF exposure (3, 5 μM) and (6, 20 μM). Areas (white arrow) become faint and areas (yellow arrow) almost disappeared after 30 min of RF exposure.

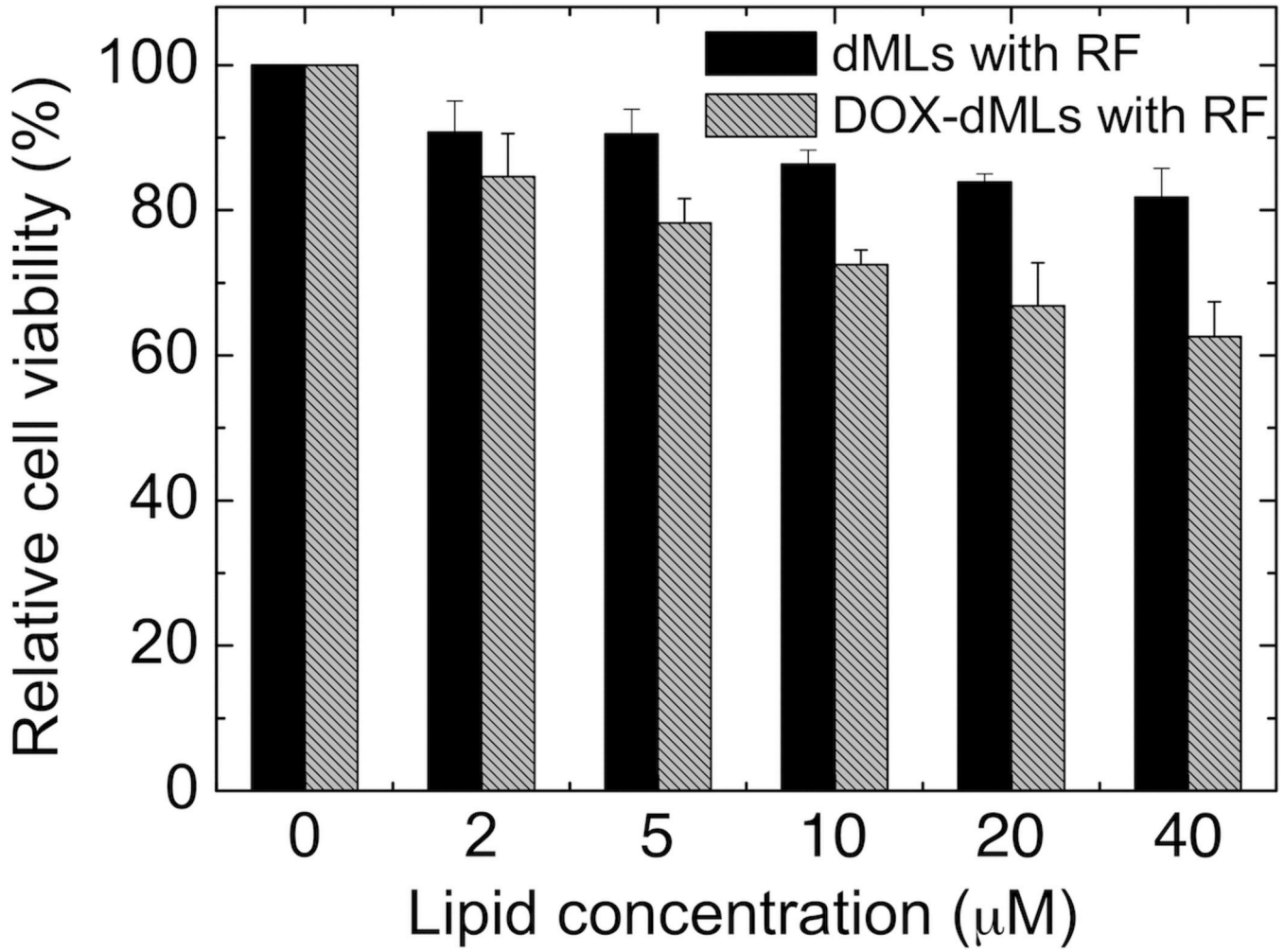

Figure 6.

Comparative cytotoxicity of dMLs and DOX-loaded dMLs with RF exposure. The cells were incubated for 3 h with dMLs, rinsed, and exposed to 30 min of RF-heating. MTT assays were conducted after 8 h incubation following the treatment. Error bars represent standard deviation for n = 16.